RSC Advances

PAPER

View Article Online
View Journal | View Issue

Cite this: RSC Adv., 2016, 6, 73887

Catalytic activity of mesoporous Ni/CNT, Ni/SBA-15 and (Cu, Ca, Mg, Mn, Co)–Ni/SBA-15 catalysts for CO_2 reforming of CH_4

Yong-Ming Dai,[a] Chi-Yuan Lu*[bc] and Chi-Jen Chang[c]

Received 23rd March 2016
Accepted 24th June 2016

DOI: 10.1039/c6ra07635a

www.rsc.org/advances

The CO_2 reforming of CH_4 to H_2 over a catalyst is an effective method for renewable energy generation. In this study, SBA-15 and CNT were chosen as supports for the Ni-based catalysts prepared by the impregnation method. The FESEM images demonstrated that NiO particles were rhombic and well distributed on the SBA-15 surface. The XRD patterns showed that the chemical state of Ni changed after the reforming reaction; the main crystals on the fresh and spent Ni/SBA-15 were found to be NiO and Ni^0. The catalytic performance of Ni/SBA-15 in CO_2/CH_4 reforming was found to be superior to that of Ni/CNT. The results of the TGA and BET analysis demonstrated that spent Ni/SBA-15 (at 600 °C) showed no catalytic decay as an insignificant amount of coke was deposited on the catalyst supports. Moreover, Ni-based bimetallic catalysts were studied for the reforming reaction, and the activity of the catalysts with respect to metals was observed to follow a particular order: Cu–Ni > Mg–Ni > Co–Ni > Ca–Ni > Mn–Ni. The Cu–Ni/SBA-15 catalyst exhibited higher catalytic activity at a reaction temperature of 650 °C as compared to the others; the H_2 yield (40%) was not decreased as the reaction time increased, and the conversion of CO_2 and CH_4 is 77% and 75%, respectively.

1. Introduction

In recent years, considerable attention has been paid to CO_2 and natural gas because of their contribution to the global greenhouse effect. In order to compensate for the effects of natural gases, processes have been developed for producing energy by the regeneration of CH_4, H_2, CH_3OH, and synthesis gases using CO_2. For instance, CO_2 reforming of CH_4 using catalysts has generally been considered as an effective method for hydrogen energy production.

Noble metal and Ni-based catalysts have long been used in the CO_2 reforming reaction; however, these catalysts have some drawbacks in the reaction, such as a high energy cost, low thermal stability of metallic sites, and low selectivity and lead to coke deposition on the catalysts.[1] Thus, new types of reforming catalysts have been studied to improve the CO_2 reforming efficiency, such as, $Ni/AlPO_4$,[2] $Ca–Ni/\alpha\text{-}Al_2O_3$,[3] $Pd\text{-}CeO_x/\alpha\text{-}Al_2O_3$,[4] Rh/Al_2O_3,[5] Ni/Mg/Al/Ce mixed oxides,[6] $Ni/Ce–ZrO_2$,[7] $Ni/Pt/\alpha\text{-}Al_2O_3–ZrO_2$,[8] Ni/SiO_2,[9] and $Pt/ZrO_2/Al_2O_3$.[10] Hou *et al.*[3] found that small amounts of Ca increased the activity and stability of $Ni/\alpha\text{-}Al_2O_3$ and that Ca improved the dispersion of Ni, strengthened the interaction between Ni and Al_2O_3, and retarded the sintering. Laosiripojana *et al.*[7] reported that Ce–ZrO_2 with a Ce/Zr ratio of 3/1 exhibited the best catalytic performance in terms of activity and stability. Further, Pompeo *et al.*[8] indicated that in systems containing ZrO_2 the deactivation levels were observed to be the lowest for Ni and Pt supported on $\alpha\text{-}Al_2O_3–ZrO_2$ because these catalysts inhibited the reactions that lead to carbon deposition.

These studies demonstrated that CO_2 reforming efficiency is enhanced when a good dispersion of the metallic active sites, thermal stability and low carbon deposition is obtained in the reaction. Superior reforming performance was observed when Ni-based catalysts were used at high temperatures above 800 °C. In order to reduce the energy required for the reforming reaction, the choice of the support is important. Earlier studies have reported that the use of mesoporous materials as catalyst support significantly enhances catalytic activity by allowing macromolecules to penetrate and be easily adsorbed onto the surface of the catalyst.[11,12] Recently, ordered mesoporous silica, SBA-15, has been used for catalytic oxidation and adsorption at low temperatures.[13,14]

Studies have been conducted on the use of SBA-15 as a catalyst support as it exhibits uniform nano-pore channels, a high specific surface area (500–800 $m^2\ g^{-1}$), and a large pore volume (0.5–1.0 $cm^3\ g^{-1}$) and is chemical inert and thermally and chemically stable.[15,16] This study aims to employ the SBA-15 as a support for the Ni-based catalyst and evaluate the catalytic activity for $CO_2–CH_4$ reforming at lower temperature. The

[a]Department of Science Education and Application, National Taichung University of Education, Taichung 403, Taiwan
[b]Department of Public Health, Chung Shan Medical University, Taichung 402, Taiwan
[c]Department of Family and Community Medicine, Chung Shan Medical University Hospital, Taichung 402, Taiwan. E-mail: cylu2280@csmu.edu.tw; Fax: +886-4-24730022 ext. 12182; Tel: +886-4-23248179

catalytic performance of Ni/SBA-15 in CO_2–CH_4 reforming is compared with that of Ni/carbon nanotube (CNT). Then, SBA-15 supported Ni-based bimetallic catalyst were studied for CO_2–CH_4 reforming with 360 min reaction time.

2. Experiment

2.1. Preparation of catalysts

Both of SBA-15 and CNT were used as supports in this study. SBA-15 was obtained using a triblock copolymer-Pluronic P123 ($EO_{20}PO_{70}EO_{20}$, Aldrich) and tetraethyl orthosilicate (98%, Aldrich) under acidic conditions (HCl, 2 M) following the hydrothermal method reported in our study (Chuang *et al.*, 2010). The CNTs were synthesized from the 3 wt% Fe/Al_2O_3 supported catalyst by the chemical vapor deposition (CVD) method at 800 °C with C_2H_2 ($H_2 : C_2H_2 = 6 : 1$) for 1 h study. Then the CNT were soaked in the acidic solution for 24 h to remove Fe and followed by washed and dried at 100 °C.

In this experiment, the nominal Ni loading weight on the support was 20 wt% for Ni/CNT and Ni/SBA-15. For Ni-based bimetallic catalysts, the loading weight of Ni and secondary metal (Cu, Ca, Mg, Mn, Co) is 10 wt% and 10 wt%, respectively. All the catalysts were introduced by excess-solution impregnation using metal nitrate as precursor. During the impregnation, the solutions (3.0 g SBA-15 and 3.0 g CNTs were added in the precursor contained-distilled water, respectively) were heated at 70 °C and constantly stirred until totally evaporated. Afterwards, Ni/CNT, Ni/SBA-15, and (Cu, Ca, Mg, Mn, Co)–Ni/SBA-15 catalysts were obtained with dried at 100 °C and then calcined at 450 °C.

2.2. CO_2 reforming of CH_4 test

Catalytic activity measurements for the CO_2 reforming of CH_4 were conducted at atmospheric pressure in a micro-catalytic reactor of quartz tube under a steady-state condition. The concentration ratio of CO_2/CH_4 was 1, and the reactions were reformed from 600 to 700 °C. Each catalyst was packed in a straight-tube reactor. A thermocouple was placed in the center of catalyst bed to record the reaction temperature and was also used to control the furnace. The reactant flows were adjusted to the volume hour space velocity (SV) of 5000–20 000 h^{-1} under atmospheric pressure. The reactants and products were monitored by an online gas chromatograph/thermal conductivity detector (Agilent GC 7890N). Thus, the conversion was calculated based on the inlet and outlet concentrations of the reactants and products.

2.3. Characterization of catalyst

An X-ray powder diffractometer (XRD) (SIEMENS D5000) was used to identify the crystalline species of Ni/SBA-15 and Ni/CNT catalysts. The powdered samples were pressed onto suitable holders. The scanning range of 2θ was from 1° to 5°and from 20° to 80°, respectively; and the scanning speed was 2° min^{-1}. XRD patterns were manually analyzed with the Joint Committee of Powder Diffraction Standard card (JCPDS). Transmission electron microscope (TEM) observations were made with a JEOL microscope (JEM-1200CXII) operated at 120 keV to observe the pore structure of SBA-15. SBA-15 was suspended in ethanol with ultrasonic. Then, a droplet was deposited on a copper grid supporting a perforated carbon film. Ni particle size, morphologies, and dispersion of metallic active phases were investigated using field emission scanning electron microscopy (FESEM; Model JSM-6700F, JEOL). The samples were immobilized on the copper holder with the carbon glue. Before analysis, the holder with samples was pretreated at 200 °C. The Brunauer–Emmett–Teller (BET) surface area of the supports and Ni catalysts was measured at 77 K by gravimetric methods with a BET-201-AEL apparatus. The BET surface area was calculated from the adsorption isotherm, and the ratio of pore volume and the average pore diameter was obtained from the pore size–volume distribution. An STA 6000 simultaneous thermal analyzer (PerkinElmer, USA), controlling thermogravimetric analysis (TGA), was used identify the thermal stability of the materials from room temperature to 900 °C with the rate of 10 °C min^{-1} under air atmosphere.

3. Results and discussion

3.1. Porous structure of SBA-15

The SBA-15 structure was observed by FESEM and TEM. Fig. 1(a) and (b) show the surface morphologies of SBA-15, as observed from the FESEM images. SBA-15 was found to have a pillar-like structure (1.5–4 μm). The FESEM images obtained at a high magnification of ×150 000 clearly showed uniform pore channels on the SBA-15 surface.

Fig. 2(a) and (b) show the TEM images of the SBA-15. These images clearly show that the pores have a well-ordered hexagonal structure (two-dimensional, *P6mm*), and pore channels have uniform diameters of 4–5 nm. The thickness of pore wall is estimated to be 3–4 nm from the black-white contrast in the

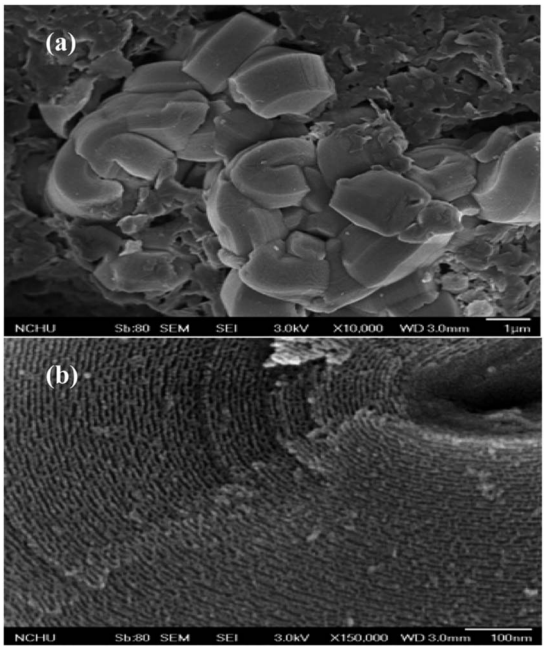

Fig. 1 FESEM images of SBA-15 support.

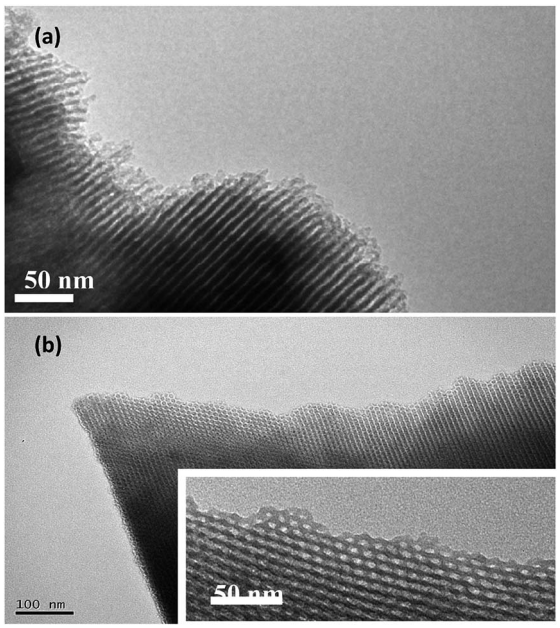

Fig. 2 TEM images of SBA-15 support.

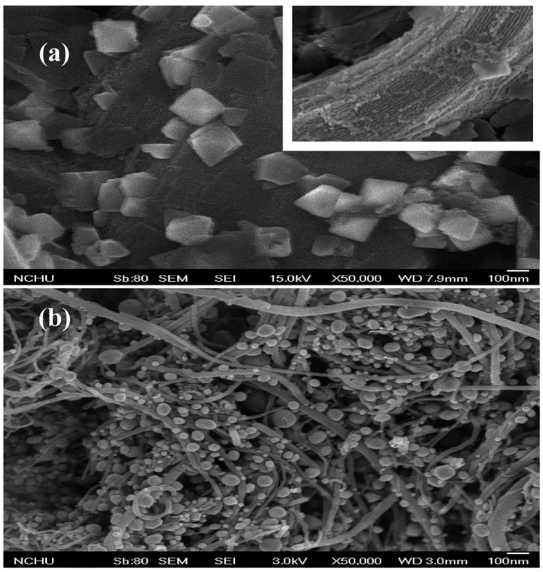

Fig. 3 FESEM images of Ni catalysts: (a) Ni/SBA-15, (b) Ni/CNT.

TEM image (Fig. 2(b)). The observed well-arrayed pore channel structure of SBA-15 is in agreement with previous studies.[15,16] Table 1 lists the values of the BET surface area and the structural characteristics of SBA-15 and CNT. SBA-15 shows a larger surface area and pore volume (532.3 $m^2 g^{-1}$, 0.61 $m^3 g^{-1}$) than CNT (65.1 $m^2 g^{-1}$, 0.44 $m^3 g^{-1}$). On the other hand, CNT shows a larger pore diameter (76.4 Å) than SBA-15 (45.9 Å).

3.2. Morphologies of Ni/SBA-15 and Ni/CNT

The surface morphologies of Ni/SBA-15 and Ni/CNT, specifically, the distributions of the Ni particles on the catalyst supports, observed by FESEM are shown in Fig. 3(a) and (b), respectively. Interestingly, the Ni particles on the two supports are observed to be of different types: the Ni particles supported on SBA-15 have a rhombic shape while those supported on CNT are spherical. In the case of Ni/SBA-15, Ni particles appear to be inserted into SBA-15. Further, from Fig. 3(a) and 1(b), a few meal phases are also found to be deposited along the pore channels of SBA-15. Comparing Ni/CNT (Fig. 3(b)) with the earlier study,[18] the spherical shapes of Ni particles were always appeared on the carbon-based supports. This finding suggests that the shape the Ni particles is influenced by the type of the support in the impregnation process. The size of Ni particles is in the range of 20–70 nm, and the average size of the Ni particles in Ni/CNT is smaller than that in Ni/SBA-15.

In order to confirm the dispersion of the Ni active phase and the variation in the catalyst support structure, a BET analysis of fresh Ni catalysts was conducted; the results of this analysis are given in Table 1. The analysis results demonstrate that Ni/SBA-15 and Ni/CNT were all mesoporous catalysts (the mesoporous volume is greater than 80% of the total volume). The results also demonstrated that the BET surface area of SBA-15 is reduced from 532.3 to 337.7 $m^2 g^{-1}$ after SBA-15 is loaded with 20 wt% Ni. The BET surface area of CNT is also observed to slightly reduce from 65.1 to 53.3 $m^2 g^{-1}$ when loaded with the same. In contrast, the total pore volume and pore diameter of SBA-15 increase from 0.61 to 0.66 $m^3 g^{-1}$ and from 45.9 to 78.7 nm, respectively. The average pore diameter of CNT catalyst increases as well, from 76.4 to 119.3 nm. According to Agnihotri *et al.*,[17] this is because the BET surface analysis of the catalysts is conducted over four areas: inside the pore channels; on the interstitial channels between the supports; on the outer groove

Table 1 BET surface area and structural characteristics of the fresh and spent Ni catalysts[a]

				Ratio of pore volume (%)		
Samples	S_{BET} ($m^2 g^{-1}$)	D_{BJH} (Å)	V_{BJH} ($m^3 g^{-1}$)	V_{micro} (<2 nm)	V_{meso} (2–50 nm)	V_{macro} (>50 nm)
SBA-15	532.3	45.9	0.61	17	82	1
Ni/SBA-15-fresh	337.7	78.7	0.66	11	88	1
Ni/SBA-15-spent	301.9	68.6	0.52	11	88	1
CNT	65.1	76.4	0.44	22	70	8
Ni/CNT-fresh	53.3	119.3	0.16	5	84	11
Ni/CNT-spent	47.9	123.6	0.15	3	87	10

[a] S_{BET} = BET surface area; D_{BJH} = BJH pore diameter and V_{BJH} = total BJH pore.

sites where the two supports meet; and on the external surface of the supports. The deposition of Ni particles on the supports increases the pore diameter of the Ni catalysts. The Ni particles were found to be well distributed on both the CNT and SBA-15 catalyst. The maintenance of ordered hexagonal arrangement of the SBA-15 frameworks upon Ni particles introduction is further supported by the N_2-adsorption data. Although the incorporation of Ni particles into SBA-15 led to a continuous decrease of the specific surface area and the cumulative pore volume, high surface areas and pore volumes as well as very narrow pore-size distributions are observed in SBA-15-supported materials with Ni particles. A similar decrease of the BET and pore volume has already been reported by Berndt *et al.* for mesoporous V-containing MCM materials.[18] Thus, it can be concluded that well-organized mesoporous SBA-15 catalysts with a high surface area could be obtained at all Ni loadings in the present study.

3.3. XRD analysis of Ni/SBA-15 and Ni/CNT

XRD analysis was conducted on both the catalysts at $2\theta = 20$–$80°$ to study the crystal phases of Ni. Fig. 4 shows the XRD patterns of fresh and spent Ni catalysts. In the case of Ni/SBA-15, the main crystal peaks of NiO were observed at $2\theta = 37.3°$ (111), 43.4° (200), 62.9° (220), 75.5° (311) after Ni impregnation on SBA-15, as shown in Fig. 4(a). The mean NiO particle size can be calculated in terms of the grain diameter D (nm) from the NiO (111) peaks ($2\theta = 37.3°$) using the Scherrer equation written as:

$$D = \frac{K\lambda}{B_{1/2}\cos\theta} \quad (1)$$

where K is a constant with a value of 0.89 and λ is the wave function, 0.154056 nm (Cu/K-alpha1). $B_{1/2}$ is the half-intensity width of the relevant diffraction peak and θ, the angle of diffraction. The mean NiO particle size of the catalyst is thus calculated as 20.3 nm. Next, small-angle XRD ($2\theta = 1$–$5°$) was employed to analyze the structure of the SBA-15 supports; the XRD results are shown in Fig. 4(b).

These results shows three well-defined peaks at 2θ values of 1–3°; these peaks are indexed as (100), (110), and (200) reflections for the pores with a hexagonal straight pores *P6mm* straight structure.[19] The small-angle XRD patterns further show that the mesoporous structure of supports stabilizes after impregnation. Next, we analyzed the XRD patterns of the fresh Ni/SBA-15 catalysts; the SBA-15 support was found to be thermally stable after calcination with active Ni at 450 °C, as evidenced by retention of the three well-defined peaks. The intense (100) peak reflects a d spacing of 81.5 Å, which corresponds to a large unit-cell parameter ($a_0 = 94.1$ Å). The value of a_0 can be calculated by an equation devised in a previous study:[20]

$$a_0 = \frac{d(100) \times 2}{\sqrt{3}} \quad (2)$$

Next, the wall thickness was calculated as 48.2 Å by the following equation:

$$\text{Wall thickness} = a_0 - \text{poresize} \quad (3)$$

The calculated wall thickness of SBA-15 is found to be larger than the observed wall thickness (Fig. 2). Further, from the values listed in Table 1, the pore size of SBA-15 calculated using the Barrett–Joyner–Halenda (BJH) method in the BET analysis is significantly smaller than the repeat distance determined by XRD; this is because the latter value includes the thickness of the pore wall. Since the wall thickness is large, the structure of SBA-15 would not be affected or destroyed easily, the reported that the use of mesoporous SBA-15 silica as a support can allow the generation of a highly efficient VO_x–SBA-15 catalyst exhibiting high selectivities (80%) to olefins at high propane conversions (42%) in the oxidative dehydrogenation of propane.[21] In the case of Ni/SBA-15, the pore volume and pore diameter were not reduced after impregnation and calcination, as given in Table 1. The results demonstrate that the SBA-15 structure remained stable in spite of the impregnation of 20 wt% Ni. In the case of Ni/SBA-15, the pore volume and pore diameter were not reduced after impregnation and calcination, as given in Table 1. The results demonstrate that the SBA-15 structure remained stable in spite of the impregnation of 20 wt% Ni.

The XRD patterns of the Ni/CNT catalyst are shown in Fig. 4(c). The peaks occurring at $2\theta = 27.2°$ and 43.3° can be attributed to the graphite structure of the CNT supports with (002) and (100) graphitic planes. Characteristic peaks of Ni^0 in the Ni/CNT catalyst were observed at $2\theta = 44.6°$ (111), 51.9° (200), and 76.4° (220) after catalyst preparation. The mean Ni^0 particle size D can be calculated from the NiO (111) peak at $2\theta = 44.6°$. The Ni^0 particle size of the catalyst is calculated as 14.0 nm. The particle size of the active phase over Ni/SBA-15 or Ni/CNT calculated from the XRD analysis results (Fig. 4) is

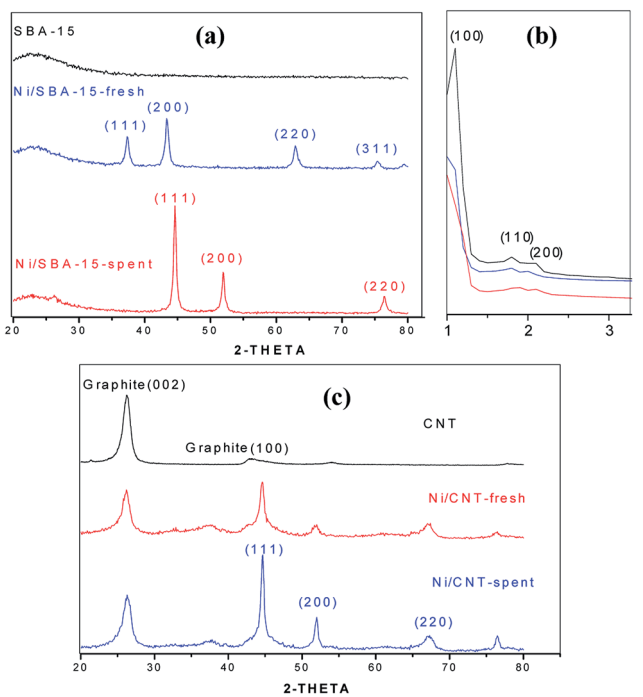

Fig. 4 XRD patterns of Ni catalysts.

found to be smaller than the particle size observed in the FESEM images (Fig. 3). The XRD patterns of Ni/SBA-15 catalyst suggest that two possible types of active phases appear on the SBA-15 support; one is rhombic, and the other is deposited along the pore channel, as shown in Fig. 4(a). Moreover, the XRD patterns show that the main crystal phase of Ni/SBA-15 and Ni/CNT is NiO and Ni^0, respectively. It is hence found that the types of Ni crystal phase is related to the shape of metal Ni (spherical and rhombic) on the support, as shown in Fig. 3.

3.4. XPS analysis of Ni/SBA-15 and Ni/CNT

XPS is a useful surface chemical analysis technique that is used to determine the species and chemical states of the elements on the surfaces of the materials. Fig. 5 shows the XPS spectra for the two samples. As our purpose is to analyze the valence state and chemical environment of Ni element on the CNT and SBA-15 support, we put our emphasis on the electron binding energy range of 850–865 eV, which covers the $2p_{3/2}$ XPS spectrum of Ni element. The typical Ni peaks at 851.7–853 eV,[22] 853.6–855.5 eV (ref. 23) and 855.8–856 eV (ref. 24) from Ni, NiO and Ni_2O_3, respectively. Comparing our results with these data, we could find that for the sample Ni element on the SBA-15 support, the Ni element is still in the form of Ni phase. The Ni element on the SBA-15, the NiO is formed as a result of the NiO on SBA-15 support, since the electron binding energy of NiO $2p_{3/2}$ shifts to 857.5 eV. These results are consistent with the XRD results, indicating that the main crystal phase of Ni/SBA-15 and Ni/CNT is NiO and Ni, respectively.

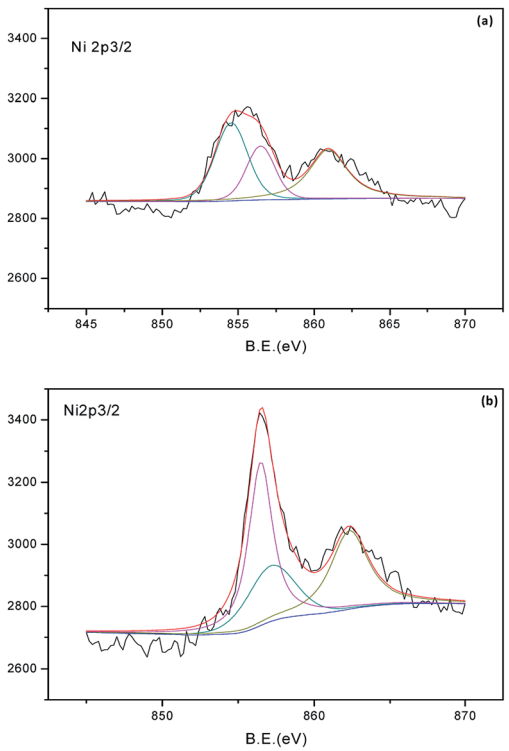

Fig. 5 The XPS spectra of (a) Ni/SBA-15, (b) Ni/CNT.

3.5. H_2-TPR analysis of Ni/SBA-15 and Ni/CNT

H_2-TPR is an efficient method to characterize the reducibility of supported nickel-based catalysts.[25,26] Fig. 6 shows the TPR spectra for the two samples. It is obvious that the H_2-TPR curves of the Ni/SBA-15 and Ni/CNT. Only two peaks appeared: one broad peak at high temperature and a shoulder peak at low temperature. Therefore, different peaks could be assigned to different interactions between the NiO and support: the first shoulder peak occurs at 250–300 °C (ref. 27) that could most likely be attributed to H_2 consumption of bulk NiO particles which has no or weak interaction with support. The second broad hydrogen consumption peaks, locating at around 310–400 °C (ref. 28) might be ascribed to the reduction of NiO and the presence of Ni-species having a lower interaction with the SBA-15 and CNT.

3.6. Comparison of the reforming reactions over Ni/SBA-15 and Ni/CNT

The CO_2–CH_4 reforming reactions over Ni/SBA-15 and Ni/CNT catalysts were studied. Fig. 7 shows the CO_2 reforming reactions at 600 °C over Ni/SBA-15 and Ni/CNT catalysts, which result in CO_2 conversion and CO production. The inlet stream comprising 10 ml CO_2 and 10 ml CH_4 was fed at a space velocity of 5000 h^{-1}. The CO yield is defined as the CO concentration in the outlet gas. The Ni/SBA-15 catalyst exhibits a more effective catalyst reforming activity (44%) than that of Ni/CNT. The primary and side reactions of CO_2–CH_4 reforming are divided in four steps:[29]

Carbon dioxide reforming: $CO_2 + CH_4 \rightarrow 2CO + 2H_2$; $\Delta H_{298} = 41$ kJ mol (a)

Reverse water-gas shift: $H_2 + CO_2 \rightarrow H_2O + CO$; (b)

Methane decomposition: $CH_4 \rightarrow C + 2H_2$; $\Delta H_{298} = 75$ kJ mol (c)

Boudouard reaction: $2CO \rightarrow C + CO_2$; $\Delta H_{298} = 171$ kJ mol (d)

For the generation of hydrogen energy, CO causes decay of the Pt electrodes in proton-exchange membrane fuel cells

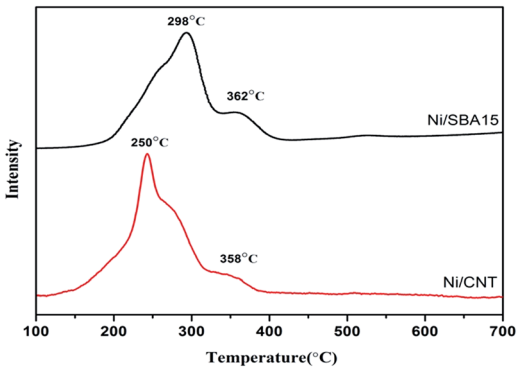

Fig. 6 H_2-TPR analysis of Ni/SBA-15 and Ni/CNT.

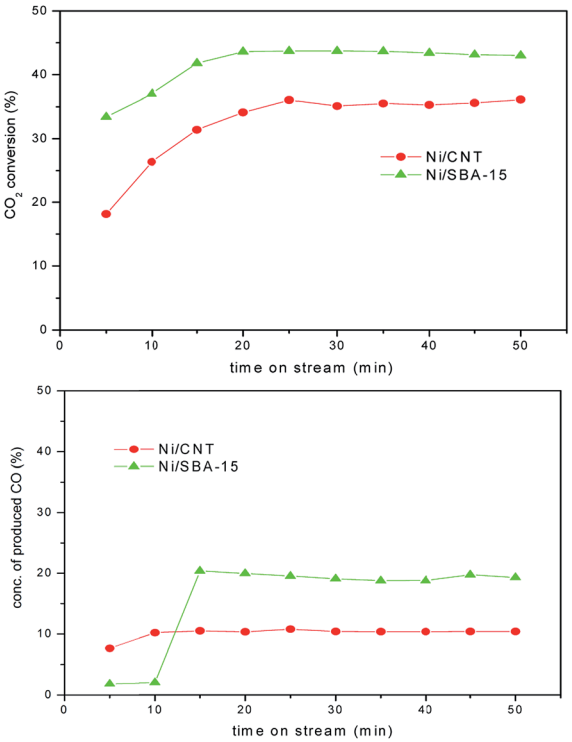

Fig. 7 CO_2 conversion and CO production over Ni/SBA-15 and Ni/CNT catalysts on reforming at 600 °C.

(PEMFCs).[30] The CO_2 reforming reaction over Ni/SBA-15 and Ni/CNT shows the concentration of produced CO is 19% and 10%, respectively. The ratio of CO production to CO_2 conversion is low but acceptable for renewable energy since more than 40% CO_2 reacted with CH_4.[3,7,8] The results indicated that CO concentration in the outlet gas is low, and the side reactions (b)–(d) could not be observed since the amount of CO produced in them is lower than the amount of CO_2 converted at 600 °C.

3.7. Characterization of spent Ni catalysts

In CO_2 reforming of CH_4, coke deposition is the main factor for catalyst decay during the reforming reaction at high temperature. The side reactions (b)–(d) are obviously not analyzed by gas chromatography. Therefore, the spent catalysts were characterized by FESEM. Fig. 8 shows the FESEM images of Ni/SBA-15 and Ni/CNT catalysts after CO_2 reforming of CH_4 over these catalysts at 600 °C. These results indicate that the maximum CO yield is 19.9% and 10.7% for Ni/SBA-15 and Ni/CNT, respectively. As observed in Fig. 8(a), the images show that the Ni particle in case of the spent Ni/SBA-15 catalyst is spherical. This shape is different from that in case of the fresh Ni/SBA-15 catalyst (Fig. 3(a)) because it changes with the chemical state after the reaction. In case of CO_2–CH_4 reforming over Ni/SBA-15, the main crystal peaks of Ni^0 in the spent Ni/SBA-15 are observed at $2\theta = 44.6°$ (111), 51.9° (200), and 76.4° (220), as shown in Fig. 4(a). The mean Ni^0 particle size can be calculated as 18.9 nm from the Ni (111) peak at $2\theta = 44.6°$. In contrast to the size, the chemical state and shape of the Ni particles did not

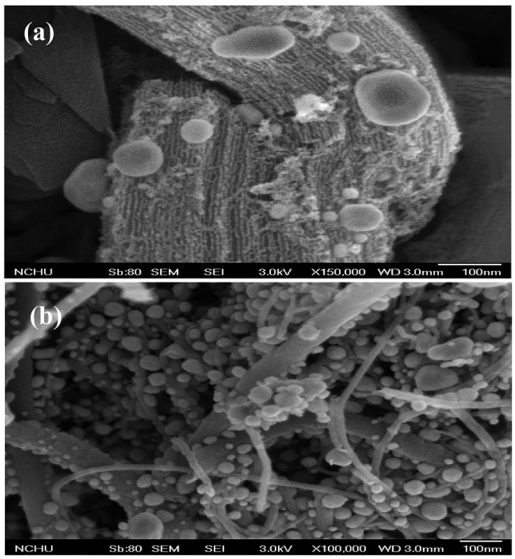

Fig. 8 FESEM images of Ni catalysts on CO_2 reforming of CH_4 reaction at 600 °C: (a) Ni/SBA-15, (b) Ni/CNT.

change after the reaction. Further, a negligible amount of coke was deposited on the SBA-15 or CNT catalyst support, as shown in Fig. 8. The FESEM images also confirmed that no side reactions occurred, which was obviously because of the negligible coke deposition.

Next, a thermogravimetric analysis of the fresh and spent Ni catalysts was conducted. The analysis results, shown in Fig. 9, demonstrate that Ni/SBA-15 and Ni/CNT provided good thermal stabilization (100–800 °C). As clearly seen in Fig. 8, the first step in the weight loss of the sample could be observed from 120 °C to 180 °C, which might be attributed to the elimination of active carbonaceous species which was responsible for the formation of synthesis gas.[31] The curve initially experienced a slight rise in the region from 300 °C to 400 °C, which is probably derived from the oxidation of metallic Ni particles. The weight losses from 450 °C to 700 °C are caused by the oxidation of carbon.[32,33] It could be clearly observed that the weight loss of the total carbon amount deposition over the used Ni/SBA-15 catalyst (5.4%) and Ni/CNT catalyst (8.9%), in agreement with the results of XRD (Fig. 4).

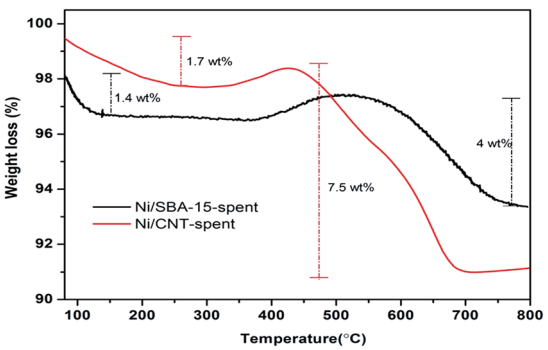

Fig. 9 TGA analysis of spent catalysts (CO_2 reforming of CH_4 reaction at 600 °C).

The XRD patterns were clearly and sharply observed because of the disappearance of impurities. The negligible amount of coke deposited on the catalyst, as found in the TGA also confirms the high thermal stabilization. However, the BET surface area, pore volume, and pore diameter of the spent catalysts (Ni/SBA-15 and Ni/CNT) are not influenced by the coke deposition or the blocking of the support pores, as shown in Table 1.

3.8. Effect of space velocity and reaction temperature on reforming reaction over Ni/SBA-15

In this study, Ni/SBA-15 is found to have better catalytic activity in a reforming reaction than Ni/CNT. Next, the optimum space velocity and reaction temperature for CO_2 reforming of CH_4 over Ni/SBA-15 were studied. Fig. 10 shows the conversions of CO_2 and CH_4 in a reforming reaction over Ni/SBA-15 at 600 °C and at different space velocities of the inlet feed stream from 5000 to 20 000 h^{-1}. It is found that both CO_2 and CH_4 conversions increased as the space velocity increases to 10 000 h^{-1}. It was considered that low space velocity inhibits the reforming reaction because of the long retention time of the reactants. However, as the space velocity increases to 20 000 h^{-1}, the conversion efficiency of CO_2 decreases, although it is still better than the CO_2 conversion efficiency at the space velocity of 5000 h^{-1}. On the other hand, CH_4 conversion is lowest (55%) at the space velocity of 20 000 h^{-1}. Under high space velocity, the reactant gases had less time to adsorb and react with the catalyst, thus leading to low efficiency of CO_2 and CH_4 conversion efficiency. Considering both the CO_2 conversion and CH_4 conversion performances, Ni/SBA-15 exhibits optimum catalytic activity at the space velocity of 10 000 h^{-1} which corresponds to 63% CO_2 conversion and 59% CH_4 conversion.

In the next experiment, an inlet stream comprising 20 ml CO_2 and 20 ml CH_4 was fed at a space velocity of 10 000 h^{-1}. Fig. 11 shows the conversions of CO_2 and CH_4 in the reforming reaction over Ni/SBA-15 at different reaction temperatures. The CO_2 and CH_4 conversions did not increased with the reaction temperature up till 650 °C. When the temperature was increased from 650 to 700 °C, both CO_2 and CH_4 conversions increased arrived at 80%. These results demonstrated that the Ni/SBA-15 conversion efficiency increases with the temperature increased and that Ni/SBA-15 provides good thermal stabilization at high temperature (700 °C).

3.9. H_2 production efficiency of reforming reaction over Ni/SBA-15

Fig. 12 shows the H_2 yield in the reforming reaction over Ni/SBA-15 at different reaction temperatures and a space velocity of 10 000 h^{-1}. The H_2 yield is defined as the H_2 concentration in the outlet gas. From the H_2 yield values and results of the previous experiment on the CO_2 and CH_4 conversion efficiencies, the H_2 yield from the reforming reaction is found to be directly related to the conversion of CO_2 and CH_4. The H_2 yield is 43% at the reaction temperature of 700 °C and decreases as the reaction temperature decreases from 700 °C to 600 °C. Daza *et al.*[6] studied the CO_2 reforming of methane over Ni/Mg/Al/Ce mixed oxides and found that at 700 °C, the H_2 yield is 15–29% whereas the CO_2 and CH_4 conversions are from 50–88%. Pompeo *et al.*[8] studied

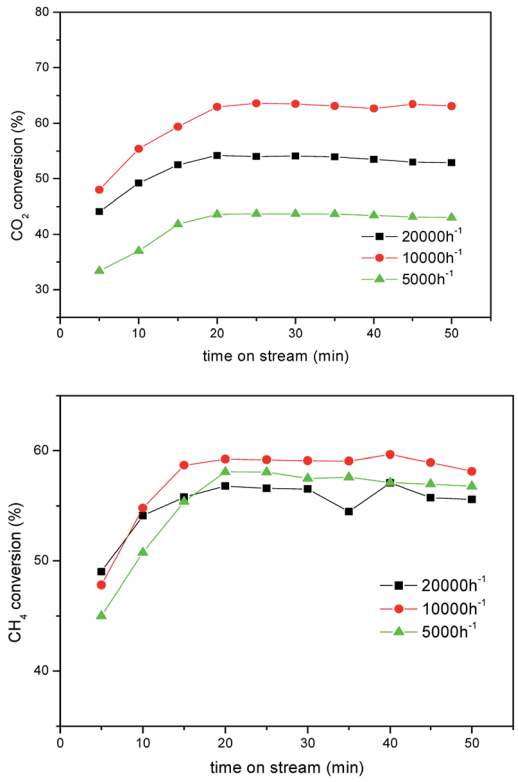

Fig. 10 The conversions of CO_2 and CH_4 over Ni/SBA-15 with different space velocity on reforming at 600 °C.

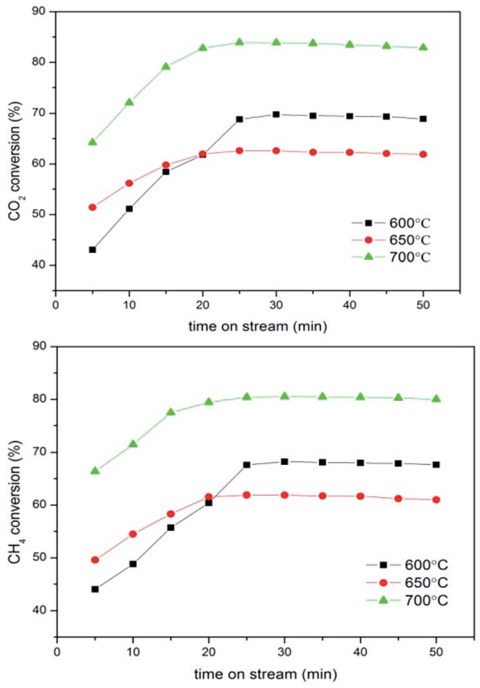

Fig. 11 The conversions of CO_2 and CH_4 over Ni/SBA-15 with different reaction temperature on reforming at a space velocity of 10 000 h^{-1}.

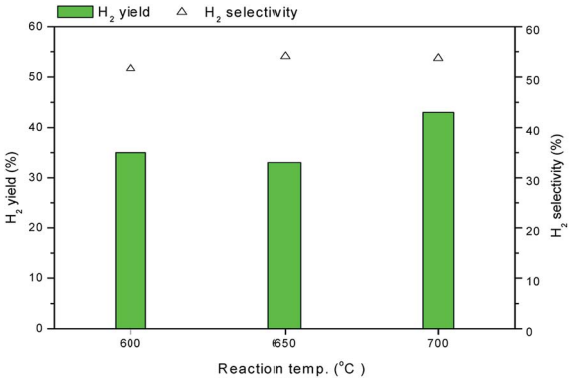

Fig. 12 H_2 yield over Ni/SBA-15 with different reaction temperature on reforming at a space velocity of 10 000 h^{-1}.

the CO_2 reforming of CH_4 at 700 °C over Ni and Pt catalysts supported on α-Al_2O_3 and ZrO_2 and found an H_2 yield of 10–40% and CO_2 and CH_4 conversions of 40–90%. In comparison with the H_2 yield with previous studies,[3,7,8] the H_2 yield obtained in this study using the Ni/SBA-15 catalyst is higher and the catalyst preparation method is simpler and less expensive.

3.10. CO_2 reforming of CH_4 over (Cu, Ca, Mg, Mn, Co)–Ni/SBA-15

In the studies above, the CO_2 reforming of CH_4 can be optimally performed over Ni/SBA-15 at 650 °C and for a 10 000 h^{-1} space velocity of the inlet feed stream. In order to reduce the energy consumption, Ni-based bimetallic catalysts, Cu–Ni/SBA-15, Co–Ni/SBA15, Mg–Ni/SBA15, Mn–Ni/SBA15, and Ca–Ni/SBA15, were studied for CO_2–CH_4 reforming, as shown in Fig. 13. Fig. 13 shows the conversions of CO_2 and CH_4 in a reforming reaction over Ni-based bimetallic catalysts at 650 °C at a space velocity of 10 000 h^{-1}. The catalyst activity for CO_2–CH_4 reforming was in the following order: Cu–Ni/SBA-15 > Mg–Ni/SBA-15 > Co–Ni/SBA-15 = Ni/SBA-15 > Mn–Ni/SBA-15 > Ca–Ni/SBA-15. These reactions of CO_2–CH_4 reforming are steps (a), (c) and (d) are strong endothermic reactions, and the C–H bond energy in methane is as high as 435 kJ mol^{-1}. The high temperature is favorable to the three reactions (a), (c) and (d). Therefore, with the reaction temperature increasing, the conversion of methane and carbon dioxide increase correspondingly. It also should be noted that Ni-based bimetallic catalysts exhibit better performance than monometallic Ni catalysts of the supports investigated.[29]

Comparing Fig. 11 with 13, Cu–Ni/SBA-15 and Mg–Ni/SBA-15 showed the better performance than that of Ni/SBA-15. The good performances over Ni-based bimetallic catalysts were suggested to be due to the electronic and geometric effects.[33] Thus, the higher catalytic reactivity of the Cu–Ni/SBA-15 and Mg–Ni/SBA-15 in better performance is due to the higher number of active sites available on the Cu–Ni/SBA-15 and Mg–Ni/SBA-15 than those on the Ni/SBA-15. This is attributed to the higher dispersion and the smaller particle size in the Cu–Ni/SBA-15 and Mg–Ni/SBA-15. Also, the smaller size and good dispersion of Ni particles may be prepared over bimetallic catalysts, as shown in TEM image of Fig. 14.

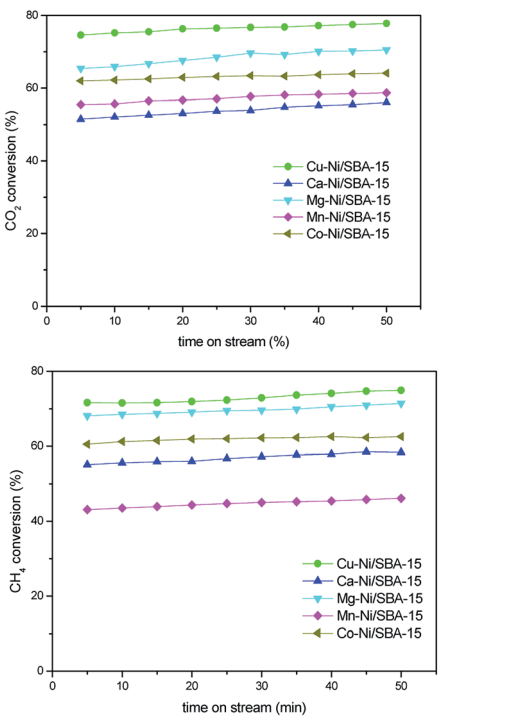

Fig. 13 CO_2 conversion and CH_4 conversion over Ni-based bimetallic catalysts on CO_2 reforming of CH_4 reaction at 650 °C at a space velocity of 10 000 h^{-1}.

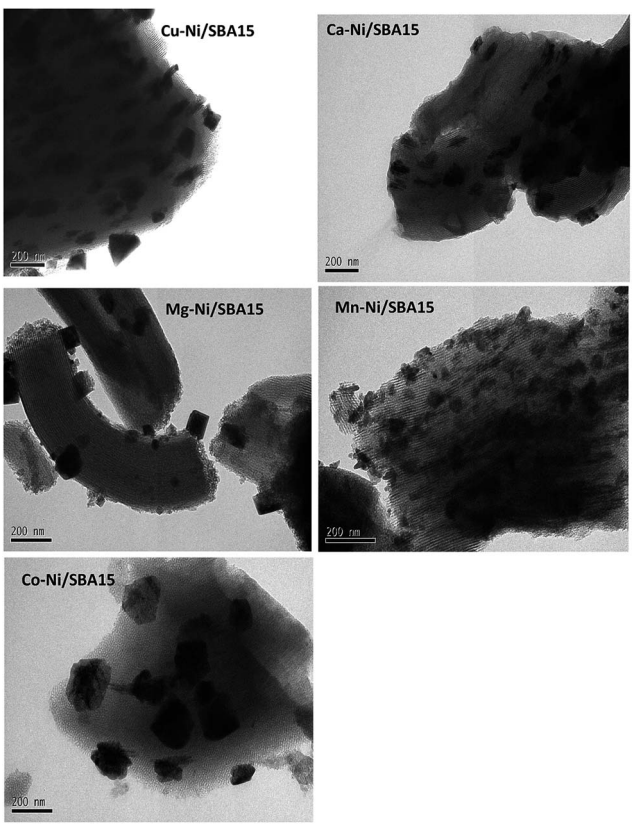

Fig. 14 TEM images of five bi-metallic supported catalysts.

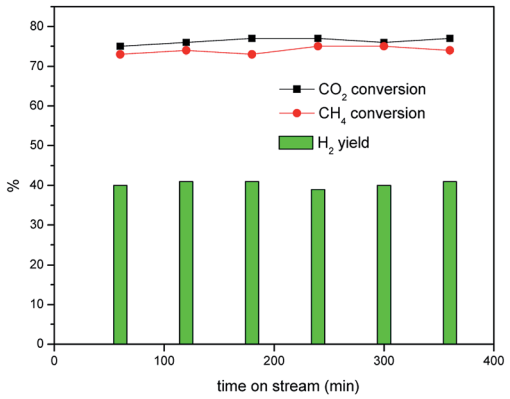

Fig. 15 CO_2 conversion, CH_4 conversion, and the H_2 yield over Cu–Ni/SBA-15 catalyst on CO_2 reforming of CH_4 reaction at 650 °C at a space velocity of 10 000 h^{-1}.

Then, Cu–Ni/SBA-15 was studied for CO_2–CH_4 reforming as a function of reaction time, as shown in Fig. 15. The experiment results showed that the conversion of CO_2 and CH_4 is 77% and 75%, respectively. Either CO_2 conversion or CH_4 conversion over Cu–Ni/SBA-15 was decreased with reaction time increased, and the H_2 yield was arrived at 40%. The results suggested that Ni-based catalyst supported on SBA-15 may not decay easily while the reaction temperature below 700 °C.

4. Conclusions

Ni-Based catalysts were prepared for use in CO_2 reforming of CH_4. The catalysts were analyzed, and it was found that Ni/SBA-15 shows better conversion efficiency than of Ni/CNT. The thickness of the SBA-15 pore wall is 48.2 Å (determined by XRD and BET analyses); this thick porous wall is suitable for catalyst preparation and the reforming reaction at high temperature. The porous structure of Ni/SBA-15 facilitates the stabilization of the reforming reaction. Moreover, (Cu, Ca, Mg, Mn, Co)–Ni/SBA-15 catalysts were also studied for CO_2–CH_4 reforming. Cu–Ni/SBA-15 catalyst exhibited higher catalytic activity at a reaction temperature of 650 °C as compared to the others. The conversion efficiency was not obviously decreased with reaction time increased; thus, SBA-15 supported bimetallic catalysts may be used as the potential material for reforming reaction at high temperature.

Acknowledgements

This work was performed under the auspices of the National Science Council of the Republic of China, under Contract MOST 97-2218-E-040-003, to which the authors wish to express their thanks.

Notes and references

1 D. Chen, R. Lødeng, A. Anundskås, O. Olsvik and A. Holmen, Deactivation during carbon dioxide reforming of methane over Ni catalyst: microkinetic analysis, *Chem. Eng. Sci.*, 2001, **56**, 1371–1379.
2 V. R. Choudhary, B. S. Uphade and A. S. Mamman, Partial oxidation of methane to syngas with or without simultaneous CO_2 and steam reforming reactions over Ni/$AlPO_4$, *Microporous Mesoporous Mater.*, 1998, **23**, 61–66.
3 Z. Hou, O. Yokota and T. Yashima, Characterization of Ca-promoted Ni/α-Al_2O_3 catalyst for CH_4 reforming with CO_2, *Appl. Catal., A*, 2003, **253**, 381–387.
4 P. G. Schulz, M. G. Gonzalez, E. Q. Quincoces and C. E. Gigola, Methane Reforming with Carbon Dioxide. The Behavior of Pd/α-Al_2O_3 and Pd-CeO_x/α-Al_2O_3 Catalysts, *Chem. Eng. Sci.*, 2005, **44**, 9020–9029.
5 M. Nagai, K. Nakahira, Y. Ozawa, Y. Namiki and Y. Suzuki, CO_2 reforming of methane on Rh/Al_2O_3 catalyst, *Chem. Eng. Sci.*, 2007, **62**, 4998–5000.
6 C. E. Daza, J. Gallego, J. A. Moreno, F. Mondragón, S. Moreno and R. Molina, CO_2 reforming of methane over Ni/Mg/Al/Ce mixed oxides, *Catal. Today*, 2008, **133–135**, 357–366.
7 N. Laosiripojana, D. Chadwick and S. Assabumrungrat, CO_2 reforming of methane over Ni/Mg/Al/Ce mixed oxides, *Chem. Eng. J.*, 2008, **138**, 264–273.
8 F. Pompeo, N. N. Nichio, M. M. V. M. Souza, D. V. Cesar, O. A. Ferretti and M. Schmal, CO_2 reforming of methane over Ni/Mg/Al/Ce mixed oxides, *Appl. Catal., A*, 2007, **316**, 175–183.
9 R. Takahashi, S. Sato, S. Tomiyama, T. Ohashi and N. Nakamura, Pore structure control in Ni/SiO_2 catalysts with both macropores and mesopores, *Microporous Mesoporous Mater.*, 2007, **98**, 107–114.
10 M. M. V. M. Souza, D. A. G. Aranda and M. Schmal, Coke Formation on Pt/ZrO_2/Al_2O_3 Catalysts during CH_4 Reforming with CO_2, *Ind. Eng. Chem. Res.*, 2002, **4**, 4681–4685.
11 C. Y. Lu, H. H. Tseng, M. Y. Wey, L. Y. Liu and K. H. Chuang, Effects of the ratio of Cu/Co and metal precursors on the catalytic activity over Cu-Co/Al_2O_3 prepared using the polyol process, *Mater. Sci. Eng., B*, 2009, **157**, 105–112.
12 C. Y. Lu and M. Y. Wey, Catalytic treating of gas pollutants over cobalt catalyst supported on porous carbons derived from rice husk and carbon nanotube, *Appl. Catal., B*, 2009, **9**, 652–661.
13 S. A. Mirji, S. B. Halligudi, N. Mathew, N. E. Jacob, K. R. Patil and A. B. Gaikwad, Adsorption of methanol on mesoporous SBA-15, *Mater. Lett.*, 2007, **61**, 88–92.
14 C. L. Peza-Ledesma, L. Escamilla-Perea, R. Nava, B. Pawelec and J. L. G. Fierro, Supported gold catalysts in SBA-15 modified with TiO_2 for oxidation of carbon monoxide, *Appl. Catal., A*, 2010, **375**, 37–48.
15 Y. J. Han, J. M. Kim and G. D. Stucky, Preparation of Noble Metal Nanowires Using Hexagonal Mesoporous Silica SBA-15, *Chem. Mater.*, 2000, **12**, 2068–2069.
16 K. H. Chuang, Z. S. Liu, Y. H. Chang, C. Y. Lu and M. Y. Wey, Study of SBA-15 supported catalysts for toluene and NO removal: the effect of promoter (Co, Ni, Mn, Ce), *React. Kinet. Catal. Lett.*, 2010, **99**, 409–420.

17 S. Agnihotri, M. Rostam-Abadi and M. J. Rood, Temporal changes in nitrogen adsorption properties of single-walled carbon nanotubes, *Carbon*, 2004, **42**, 2699–2710.

18 H. Berndt, A. Martin, A. Brückner, E. Schreier, D. Müller, H. Kosslick, G. U. Wolf and B. Lücke, Structure and catalytic properties of VO_x/MCM materials for the partial oxidation of methane to formaldehyde, *J. Catal.*, 2000, **191**, 384–400.

19 D. Zhao, Q. Huo, J. Feng, B. F. Chmelka and G. D. Stucky, Nonionic Triblock and Star Diblock Copolymer and Oligomeric Surfactant Syntheses of Highly Ordered, Hydrothermally Stable, Mesoporous Silica Structures, *J. Am. Chem. Soc.*, 1998, **120**, 6024–6036.

20 D. Zhao, J. Feng, Q. Huo, N. Melosh, G. H. Fredrickson, B. F. Chmelka and G. D. Stucky, Triblock Copolymer Syntheses of Mesoporous Silica with Periodic 50 to 300 Angstrom Pores, *Science*, 1998, **279**, 548–552.

21 Y. M. Liu, Y. Cao, K. K. Zhu, S. R. Yan, W. L. Dai, H. Y. He and K. N. Fan, Highly efficient VO_x/SBA-15 mesoporous catalysts for oxidative dehydrogenation of propane, *Chem. Commun.*, 2002, 2832–2833.

22 Y. Lu, J. Xue, C. Yu, Y. Liu and S. Shen, Mechanistic investigations on the partial oxidation of methane to synthesis gas over a nickel-on-alumina catalyst, *Appl. Catal., A*, 1998, **174**, 121–128.

23 S. R. Kirumakki, B. G. Shpeizer, G. V. Sagar, K. V. R. Chary and A. Clearfield, Hydrogenation of naphthalene over NiO/SiO_2–Al_2O_3 catalysts: structure–activity correlation, *J. Catal.*, 2006, **242**, 319–331.

24 S. Seal, S. C. Kuiry and L. A. Bracho, Studies on the surface chemistry of oxide films formed on IN-738LC superalloy at elevated temperatures in dry air, *Oxid. Met.*, 2001, **56**, 583–603.

25 Z. Xu, Y. M. Li, J. Zhang, L. Chang, R. Q. Zhou and Z. T. Duan, Ultrafine NiO–La_2O_3–Al2O3 aerogel: a promising catalyst for CH_4/CO_2 reforming, *Appl. Catal., A*, 2001, **213**, 65–71.

26 J. C. Escritori, S. C. Dantas, R. R. Soares and C. E. Hori, Methane autothermal reforming on nickel–ceria–zirconia based catalysts, *Catal. Commun.*, 2009, 1090–1094.

27 X. Y. Quek, D. P. Liu, W. N. E. Cheo, H. Wang, Y. Chen and Y. H. Yang, Nickel-grafted TUD-1 mesoporous catalysts for carbon dioxide reforming of methane, *Appl. Catal., B*, 2010, **95**, 374–382.

28 M. H. Zhou, L. F. Tian, L. Niu, C. Li, G. M. Xiao and R. Xiao, Upgrading of liquid fuel from fast pyrolysis of biomass over modified Ni/CNT catalysts, *Fuel Process. Technol.*, 2014, **126**, 12–18.

29 Z. G. Hao, Q. H. Zhu, Z. Jiang, B. L. Hou and H. Z. Li, Characterization of aerogel Ni/Al_2O_3 catalysts and investigation on their stability for CH_4–CO_2 reforming in a fluidized bed, *Fuel Process. Technol.*, 2009, **90**, 113–121.

30 H. Igarashi, H. Uchida, M. Suzuki, Y. Sasaki and M. Watanabe, Removal of carbon monoxide from hydrogen-rich fuels by selective oxidation over platinum catalyst supported on zeolite, *Appl. Catal., A*, 1997, **159**, 159–166.

31 Z. L. Zhang and X. E. Verykios, Carbon dioxide reforming of methane to synthesis gas over supported Ni catalysts, *Catal. Today*, 1994, **21**, 589–595.

32 Z. C. Liu, J. Zhou, K. Cao, W. M. Yang, H. X. Gao, Y. D. Wang and H. X. Li, Highly dispersed nickel loaded on mesoporous silica: one-spot synthesis strategy and high performance as catalysts for methane reforming with carbon dioxide, *Appl. Catal., B*, 2012, **125**, 324–330.

33 B. Coq and F. Figueras, Bimetallic palladium catalysts: influence of the co-metal on the catalyst performance, *J. Mol. Catal. A: Chem.*, 2001, **173**, 117–134.

